RSC Advances

PAPER

View Article Online
View Journal | View Issue

Cite this: *RSC Adv.*, 2019, **9**, 30752

A new way for lead–boron resin composite modification: SiO_2 coated lead powders by a sol–gel method

Lingcheng Ma,[a] Ying Liu,[ab] Jun Li,*[ab] Na Jin,[ab] Cheng Li,[a] Xue Zhou[a] and Jiaxu Ma[a]

In order to improve the composition distribution and flame retardancy of composites, the effects of silicon dioxide (SiO_2) coatings with different contents on physical properties of lead (Pb) powders and composites were investigated in this research. SiO_2 coated Pb powders (SiO_2@Pb) with contents of 0, 0.237, 0.486, 0.683, 0.967 wt% were synthesized by a sol–gel method, then mixed with boron carbide (B_4C) powders and boron phenolic resins (BPRs) to prepare SiO_2@Pb/B_4C/BPRs composites by molding. SiO_2 coating on the surface of Pb powders in flakes or islands increases the specific surface area and oxidation temperature of the SiO_2@Pb powders. For the SiO_2@Pb/B_4C/BPRs composites, the composition uniformity of composites is improved due to the reduction of the true density difference value between fillers (Pb, B_4C), which is beneficial for the physical properties of the composites. Furthermore, the mechanical properties and thermal conductivity increase with the addition of SiO_2 content, achieving a maximum value at 0.237 wt%, and then decrease gradually with a further increase of SiO_2 content. Moreover, SiO_2 coatings improve the limit oxygen index (LOI) of the composites and reduce the cracks of composites after burning. Composites with the SiO_2 content of 0.486 wt% have optimal comprehensive physical properties, where the tensile strength, bending strength, impact toughness are 42.5 MPa, 72.4 MPa, 6.5 kJ m^{-2}, respectively and the LOI is 41.8%.

Received 30th July 2019
Accepted 23rd September 2019

DOI: 10.1039/c9ra05913j

rsc.li/rsc-advances

1. Introduction

Nuclear shielding composites are important materials used for blocking γ rays and neutron radiation to ensure safety of personnel and machines.[1–5] Lead-boron polyethylene (PBPE) is widely used for nuclear shielding. The resins have good moderating effect on fast neutrons, while boron atoms can absorb thermal neutrons effectively and Pb atoms have effective shielding effect on γ rays.[6–8] However, the volume ratio of fillers (Pb, B_4C) of lead–boron resins composites is over 30% to ensure the nuclear shielding performance. There is inevitable component segregation in the composites due to the huge density difference between fillers, which has adverse effects on the comprehensive physical properties of composites and restricts their widespread application.

Up to now, the improvement of the physical properties of resin matrix composites is mainly by adding aids, such as adding flame retardants to improve the flame resistance properties of composites, adding glass fibers to increase the mechanical properties of composites, *etc.*[9,10] Regrettably, the addition of aids is generally large, which will affect composition and properties of composites and some aids (halogen flame retardants) may produce toxic gases, which are rarely used.[11–16] So far, many efforts are devoted to the study of aids but there is little literature refers to improving the physical properties and component homogeneity of composites by surface treatment of fillers.

SiO_2 is used as a potential environmental flame retardant to improve the flame resistance of composites. Some literatures indicate that SiO_2 forms SiC layers with the residual carbon layers or glassy SiO_2 layers to improve the compactness of carbon layers, which prevents the fire spread and heat transfer.[17,18] However, there are few literatures on its flame resistance mechanism in the composites containing fillers with low melting point such as Pb powders.

This paper presented the study of coating SiO_2 shell on the surface of Pb powders (SiO_2@Pb) by sol–gel method.[19] Consequently, a type of resin matrix shielding composites with high flame retardant and excellent mechanical properties was obtained with SiO_2@Pb powders, B_4C powders and BPRs. The effects of SiO_2 coatings on physical properties of powders and composites were investigated in this research. The study can provide a new way, which is modifying fillers surface, to improve the properties of composites.

[a]*College of Materials Science and Engineering, Sichuan University, Chengdu 610065, P. R. China. E-mail: abthonyli@163.com*
[b]*Key Laboratory of Advanced Special Materials and Technology Ministry of Education, Chengdu 610065, P. R. China*

2. Experimental section

2.1 Materials

Boron phenolic resins (BPRs), lead powders (Pb), boron carbide powders (B_4C), tetraethoxysilane (TEOS), NH_4OH, silane coupling agent (KH550) and other used reagents are all commercially available. All of the reagents used in these experiments are analytical grade.

2.2 Synthesis of SiO_2@Pb powders

Fig. 1a shows the schematic diagram of the synthesis of SiO_2@Pb powders. In this work, the SiO_2@Pb powders with different content of SiO_2 were synthesized by sol–gel.[20–22] The Pb powders and NH_4OH were added into alcohol–water solution (volume ratio of alcohol to water was 5 : 1) with mechanical stirring. Then the TEOS was dropped by a constant flow pump with 0.5 mL min^{-1} under 25 °C. Until the TEOS was dropped completely, the temperature was set to 80 °C to get the SiO_2@Pb slurry. Finally put the SiO_2@Pb slurry into a vacuum oven under 80 °C to remove all the solvent and get dry SiO_2@Pb powders.

2.3 Preparation of SiO_2@Pb/B_4C/BPRs composites

Fig. 1b shows the schematic diagram of the preparation of SiO_2@Pb/B_4C/BPRs composites. 15 wt% BPRs, 80 wt% SiO_2@Pb powders, 5 wt% B_4C powders and KH550 were added in alcohol and mixed by mechanical stirring for 4 h in 40 °C. Then put the SiO_2@Pb/B_4C/BPRs slurry into a vacuum oven under 110 °C and crushed to obtain raw material particles. The raw material particles were put into a hard alloy mould with cold pressing firstly and then hot pressing at 120 °C for 1 h, 150 °C for 1 h and 180 °C for 3 h to get the SiO_2@Pb/B_4C/BPRs composites.

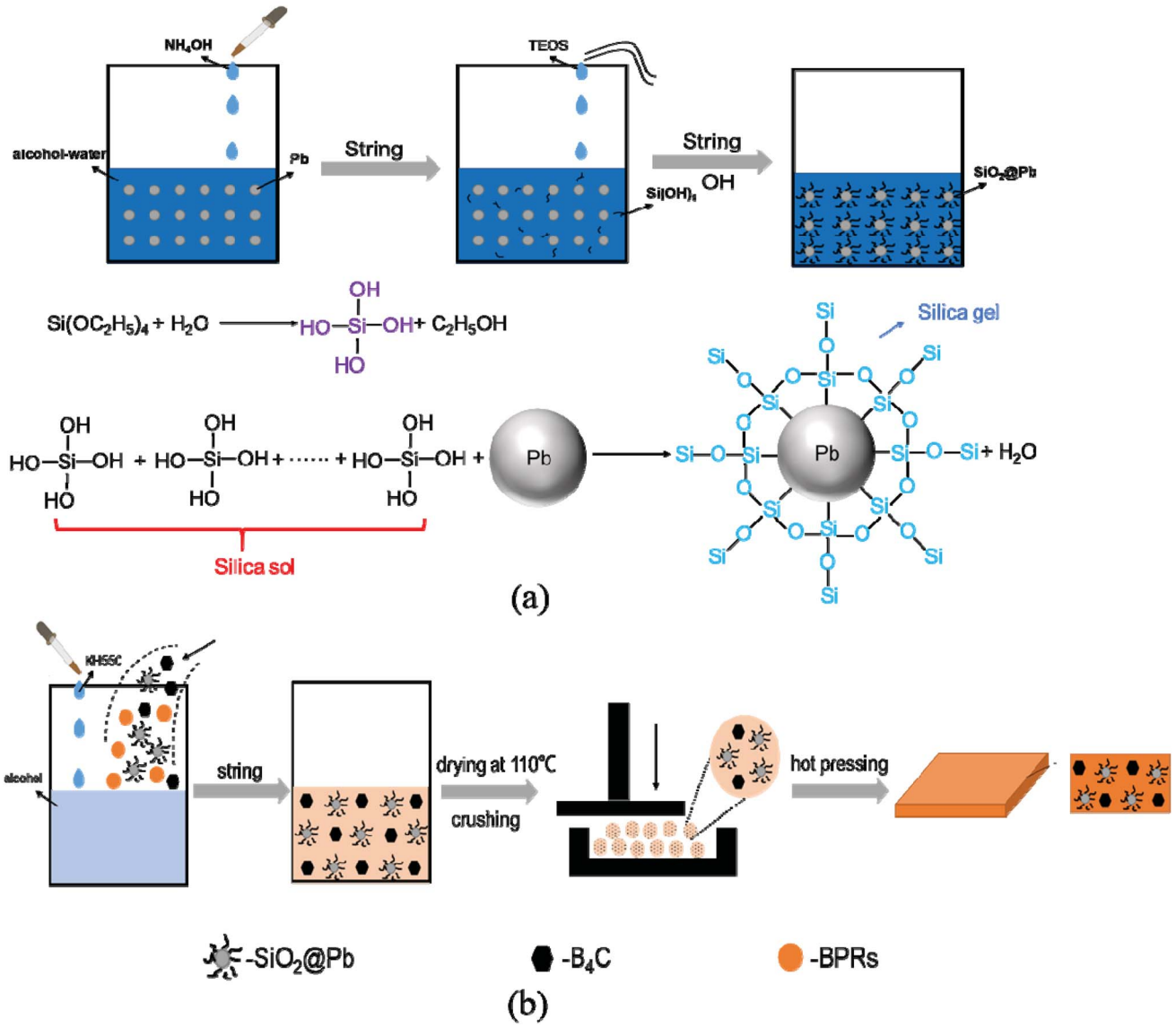

Fig. 1 (a) Schematic diagram of the synthesis of SiO_2@Pb powders; (b) schematic diagram of the preparation of SiO_2@Pb/B_4C/BPRs composites.

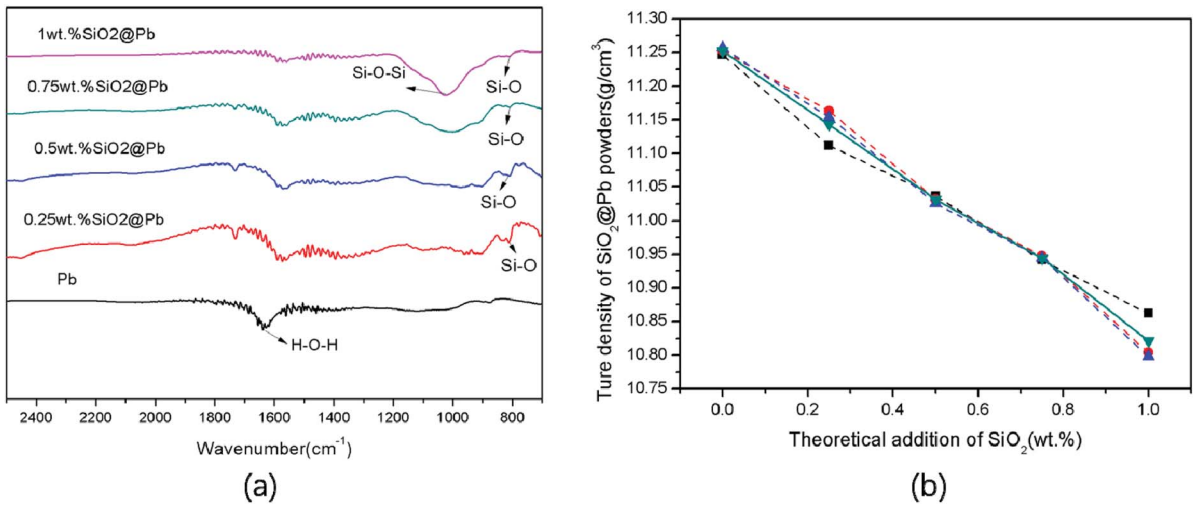

Fig. 2 (a) FI-TR spectra of SiO_2@Pb powders with different theoretical addition of SiO_2; (b) true density of SiO_2@Pb with different theoretical addition of SiO_2.

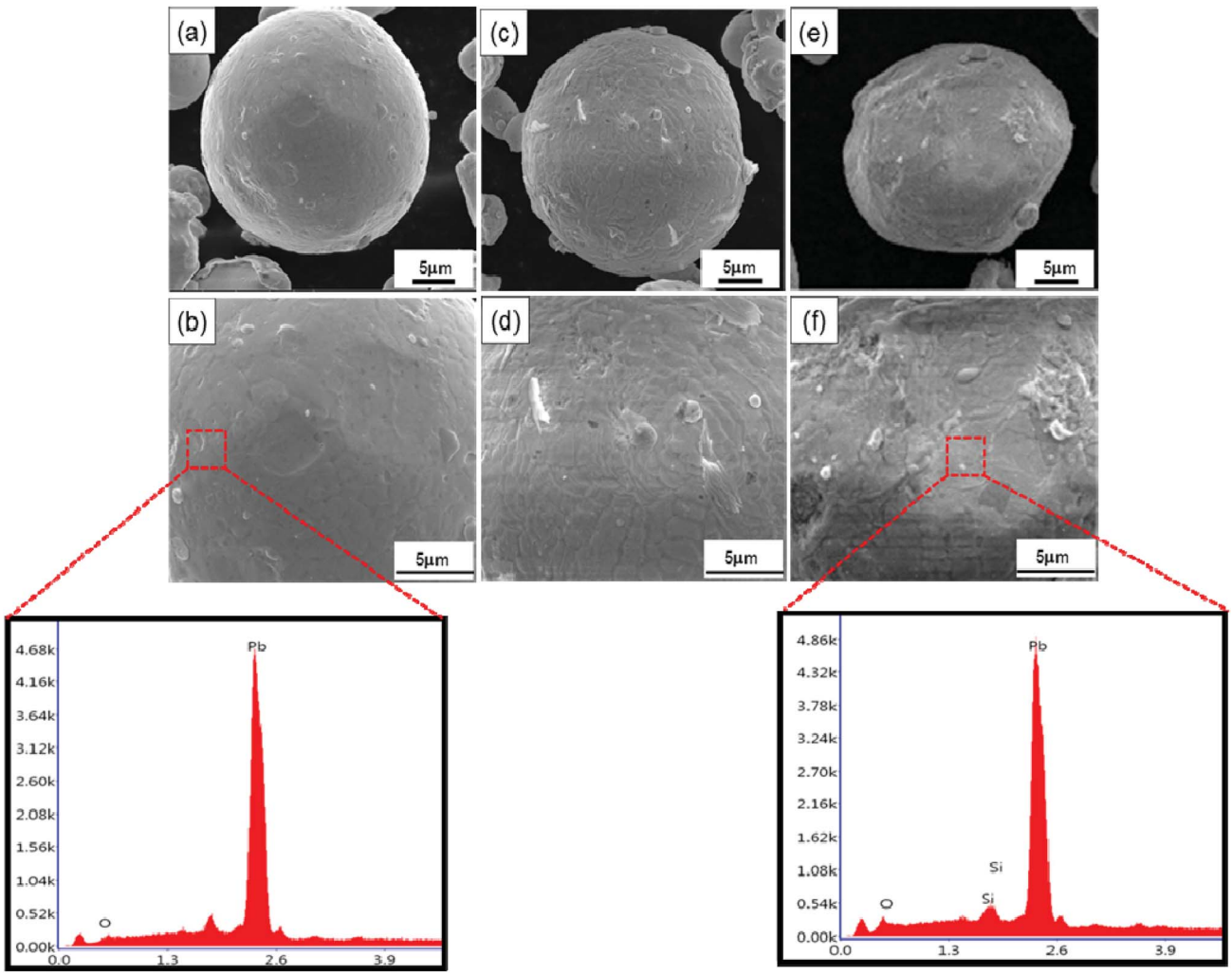

Fig. 3 SEM images and EDS of SiO_2@Pb powders with different theoretical addition of SiO_2: (a and b) Pb; (c and d) 0.486 wt% SiO_2@Pb; (e and f) 0.967 wt% SiO_2@Pb.

2.4 Measurements

The functional groups on surface of Pb powders was examined by a Nicolet IS10 Fourier transform infrared spectroscopy (FTIR) recorded between 400 and 4000 cm^{-1}. The surface morphology of SiO_2@Pb powders was observed by a scanning electron microscopy (SEM) using a field-emission scanning election microscope (FESEM, Inspect F20). The transmission electron microscope (TEM) images was tested by field-emission transmission electron microscopy (FEI Talos F200). The true density of the SiO_2@Pb powders was measured by 3H-2000 TD2 fully automatic true density analyser. The specific surface area of the SiO_2@Pb powders was measured by a kubo-x1000 BET surface analyser. The mechanical properties of composites were tested by a Universal Material Testing Machine (Instron 4302). Thermogravimetric analysis (TGA) was performed on a DSC1/700 instrument heated from room temperature to 800 °C at a heating rate of 10 °C min^{-1} in air. The thermal conductive of the composites was tested by a TPS2500S thermal constant analyser. The LOI was performed on a JF-3 digital display oxygen index tester. The density of the composites was measured by an electronic scale (ESJ110-4A) based on Archimedes principle.

3. Results and discussion

3.1 Characterization of SiO_2@Pb powders

In this research, the theoretical addition of SiO_2 is 0.25, 0.5, 0.75, 1 wt% of Pb. Fig. 2a shows the FI-TR spectra of SiO_2@Pb powders with different SiO_2 theoretical addition. It can be seen that the asymmetrical telescopic vibration absorption peak of Si–O–Si (1041.79 cm^{-1}) and the symmetrical telescopic vibration absorption peak of Si–O (799 cm^{-1}) are indicated, which demonstrates the formation of SiO_2. Additionally, with the increase of SiO_2 content, the intensity of H–O–H (1630 cm^{-1}) recedes gradually. The phenomenon is for the reason that the SiO_2 coatings reduce the water content on the Pb powders surface as hydrophobic layers.[23]

Fig. 2b shows the true density of SiO_2@Pb powders with different theoretical addition of SiO_2. Average value of true density of SiO_2@Pb powders with 0, 0.25, 0.5, 0.75, 1 wt% theoretical addition of SiO_2 is 11.252, 11.143, 11.031, 10.944, 10.821 g cm^{-3}. According to the formula (eqn (1)),

$$\frac{x}{\rho_{SiO_2}} + \frac{1-x}{\rho_{Pb}} = \frac{1}{\rho_{SiO_2@Pb}} \quad (1)$$

where x, ρ_{SiO_2}, ρ_{Pb}, $\rho_{SiO_2@Pb}$ is the content of SiO_2, the density of SiO_2, Pb, SiO_2@Pb, respectively. Based on the theoretical density of SiO_2 (2.2 g cm^{-3}),[24] it can be obtained that the content of SiO_2 is 0.237, 0.486, 0.683, 0.967 wt%, respectively.

The SEM images and EDS of SiO_2@Pb powders are shown in Fig. 3, the result of EDS reveals that Si existed on the surface of Pb powders after surface modification. Combined with the FI-TR spectra, it can be inferred that SiO_2 coats on the surface of Pb powders by sol–gel. According to the SEM images, the SiO_2 layers increase the surface roughness of Pb powders. In addition, lamellar SiO_2 (Fig. 3d) coated on the surface of Pb powders gradually change to islands with the SiO_2 content increasing further to 0.967 wt% (Fig. 3f).

To further characterize the core–shell structure of SiO_2@Pb powders, the TEM image and energy spectrum analysis of 0.967 wt% SiO_2@Pb powders were obtained as shown in Fig. 4, Fig. 4a is the image of high-angle annular dark field (HAADF), Fig. 4b is the energy spectrum surface scanning image of Pb and Si corresponding to the HAADF imaging mode horizon. HADDF results show that there is obvious contrast difference between

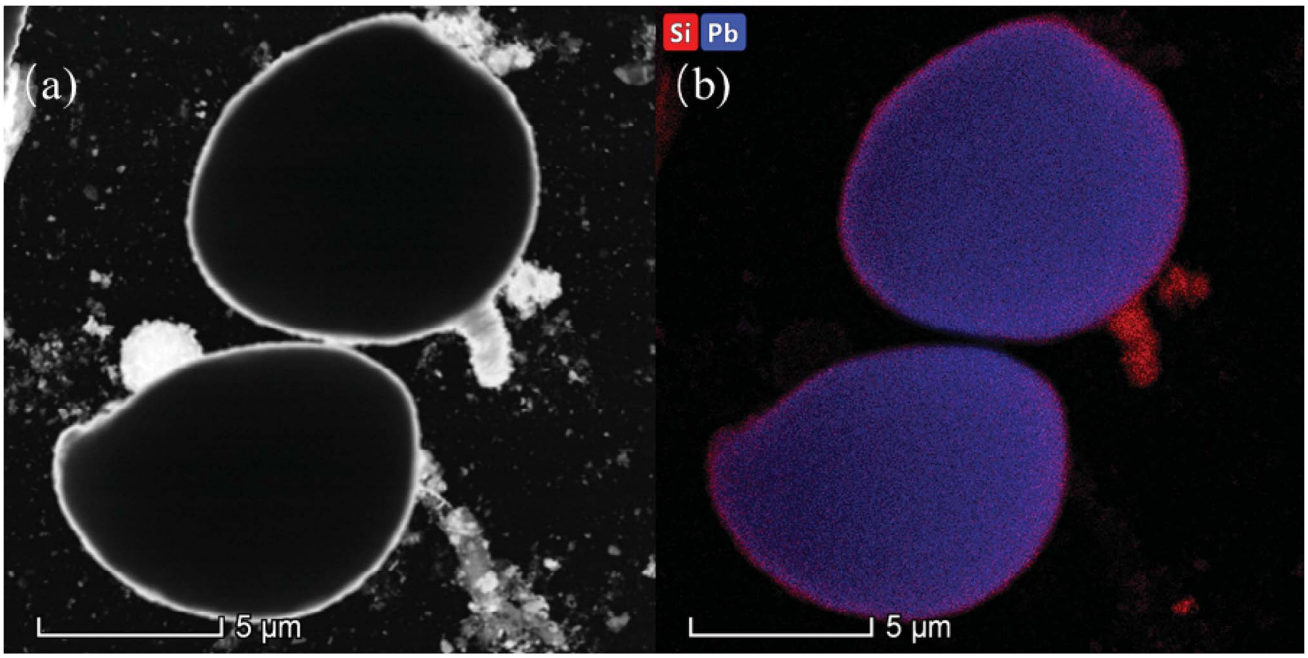

Fig. 4 TEM image and energy spectrum analysis of 0.967 wt% SiO_2@Pb powders. (a) HAADF-STEM; (b) surface scanning of Pb and Si.

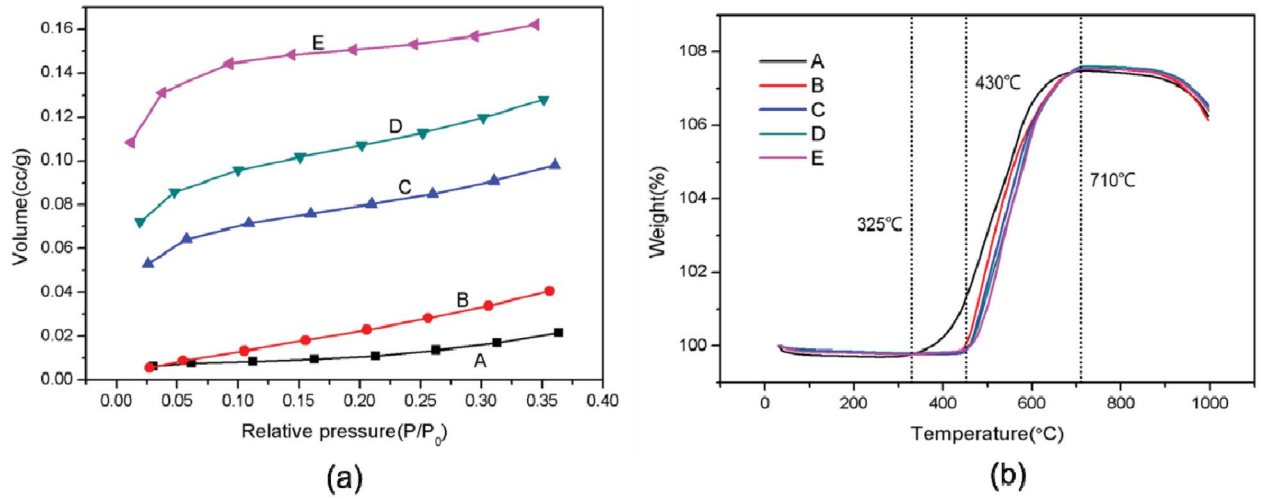

Fig. 5 (a) Nitrogen adsorption isotherm of SiO_2@Pb powders, A: Pb, B: 0.237 wt% SiO_2@Pb, C: 0.486 wt% SiO_2@Pb, D: 0.683 wt% SiO_2@Pb, E: 0.967 wt% SiO_2@Pb; (b) TGA curves of SiO_2@Pb powders, A: Pb, B: 0.237 wt% SiO_2@Pb, C: 0.486 wt% SiO_2@Pb, D: 0.683 wt% SiO_2@Pb, E: 0.967 wt% SiO_2@Pb.

the outer and the core of the particles. It can be seen that the bright annular region of the outer ring is SiO_2 with smaller relative mass, and the dark circular region is Pb. Besides, the result of elemental surface scanning image is also agreement of that of HADDF, showing Si distributes in the outer ring and Pb concentrates in the central region. Therefore, the 0.967 wt% SiO_2@Pb powders show obvious core–shell structure.

For the roughening of Pb powders after modification, the BET specific surface area of SiO_2@Pb powders was also characterized. Fig. 5a is the nitrogen adsorption isotherm of SiO_2@Pb powders. With the increase of SiO_2 content, the nitrogen adsorption volume of SiO_2@Pb powders increases obviously. In addition, the left end of the curves (relative pressure: 0–0.1) approaches the *Y* axis, which indicates that the interaction force between the SiO_2@Pb powders and nitrogen increases gradually. According to the IUPAC classification, the isotherm of Pb is type III, which shows the weak adsorption between Pb powders and nitrogen. After surface modification, the isotherms change to type II or type IV.[25,26] It can be inferred that the isotherm is type IV because SiO_2 is a disordered mesoporous material.[27] The BET specific surface areas of SiO_2@Pb powders are 0.0470, 0.1324, 0.2763, 0.3654, 0.4800 $m^2\ g^{-1}$, respectively with the increase of SiO_2 content.

Fig. 5b shows the TGA curves of SiO_2@Pb powders from room temperature to 800 °C in air. After surface modification, the initial oxidation temperature of Pb powders increases from 325 °C to 430 °C. It can be attributed to the lower thermal conductivity of SiO_2 (1.03 W m^{-1} K^{-1})[28] compared with Pb (34.8 W m^{-1} K^{-1}).[29] The SiO_2 coatings act as heat insulation layers to insulate the external heat, which increases the initial oxidation temperature and delay the oxidation reaction.

3.2 Characterization of SiO_2@Pb/B_4C/BPRs composites

For the lead–boron resin matrix composites, component segregation exists in composites inevitably because of the large density difference between fillers, which causes weak shielding zones in composites and damages the physical properties of

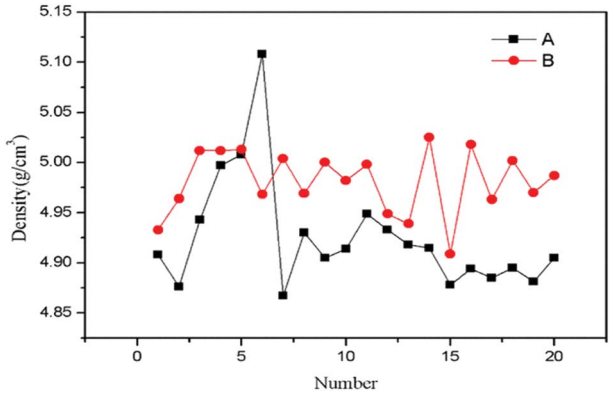

Fig. 6 Density of SiO_2@Pb/B_4C/BPRs composites in 20 regions. A: Pb/B_4C/BPRs composites; B: 0.486 wt% SiO_2@Pb/B_4C/BPRs composites.

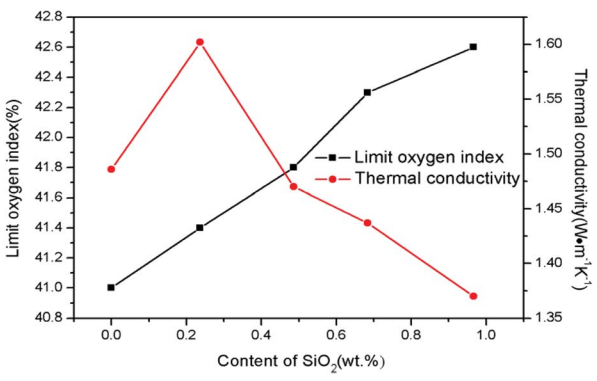

Fig. 7 LOI and thermal conductivity of SiO_2@Pb/B_4C/BPRs composites with different content of SiO_2.

composites. Thus, the composition uniformity of the 0.486% SiO_2@Pb/B_4C/BPRs composites was also analysed. Composition homogeneity in composites can be expressed by the dispersion degree of density in each region of composites. The large degree of dispersion indicates that the component segregation in the composites. Fig. 6 shows the dispersion degree of density of Pb/B_4C/BPRs composites and 0.486 wt% SiO_2@Pb/B_4C/BPRs composites in 20 regions. Eqn (2) is the standard deviation calculation formula,

$$\sigma = \sqrt{\frac{1}{N}\sum_{i=1}^{N}(x_i - \mu)^2} \quad (2)$$

In which μ is the arithmetic mean of the density. The standard deviations of Pb/B_4C/BPRs composites and 0.486 wt% SiO_2@Pb/B_4C/BPRs composites are 0.05679 and 0.03181, respectively. The result is attributed to the reduction of the true density value between 0.486 wt% SiO_2@Pb powders (11.031 g cm^{-3}) and B_4C powders (2.52 g cm^{-3}).[30] Besides, the roughening of Pb powders and plentiful –OH groups on the SiO_2 layers enhance the interfacial interaction between Pb and BPRs, which is beneficial to the dispersion of Pb powders in matrix during the mixing process.

For the further study about the SiO_2 coating effect on SiO_2@Pb/B_4C/BPRs composites, the thermal conductivity and LOI of composites were tested as shown in Fig. 7. The enhancement of interfacial interaction between Pb and BPRs reduces the interfacial thermal resistance and improved the thermal conductivity when the SiO_2 content is 0.237 wt%.[31] Then, the thermal conductivity decreases gradually with the increase of SiO_2 content. Pb powders agglomerating in SiO_2@Pb/B_4C/BPRs composites form thermal conductivity chains, which improves the thermal conductivity of composites. SiO_2 coatings insulate heat transfer due to the low powders in composites, which inhibits Pb powders forming thermal conductivity chains in the composites.

The LOI of the composites was also characterized to observe the effect of SiO_2 on the composites flame retardancy. Literatures show SiO_2 can improve the flame retardancy of composites by improve the compactness of carbon layers.[17,18] The same result is obtained in this study, where the LOI of SiO_2@Pb/B_4C/BPRs composites increases from 41% to 42.6%. SiO_2 coatings on Pb powders surface show new flame-retardant mechanism in this research as following. As shown in Fig. 8a, huge holes appear in the composites with the maximum diameter of holes about 350 μm and composites crack obviously, which promote the flame spreading to the interior of composites. The reason of the phenomenon is that fillers segregation exists in Pb/B_4C/BPRs composites. Hence, agglomerated Pb powders melt and flow, which causes holes and cracks in composites. From Fig. 8b, small Pb particles disperse in the interior of composites

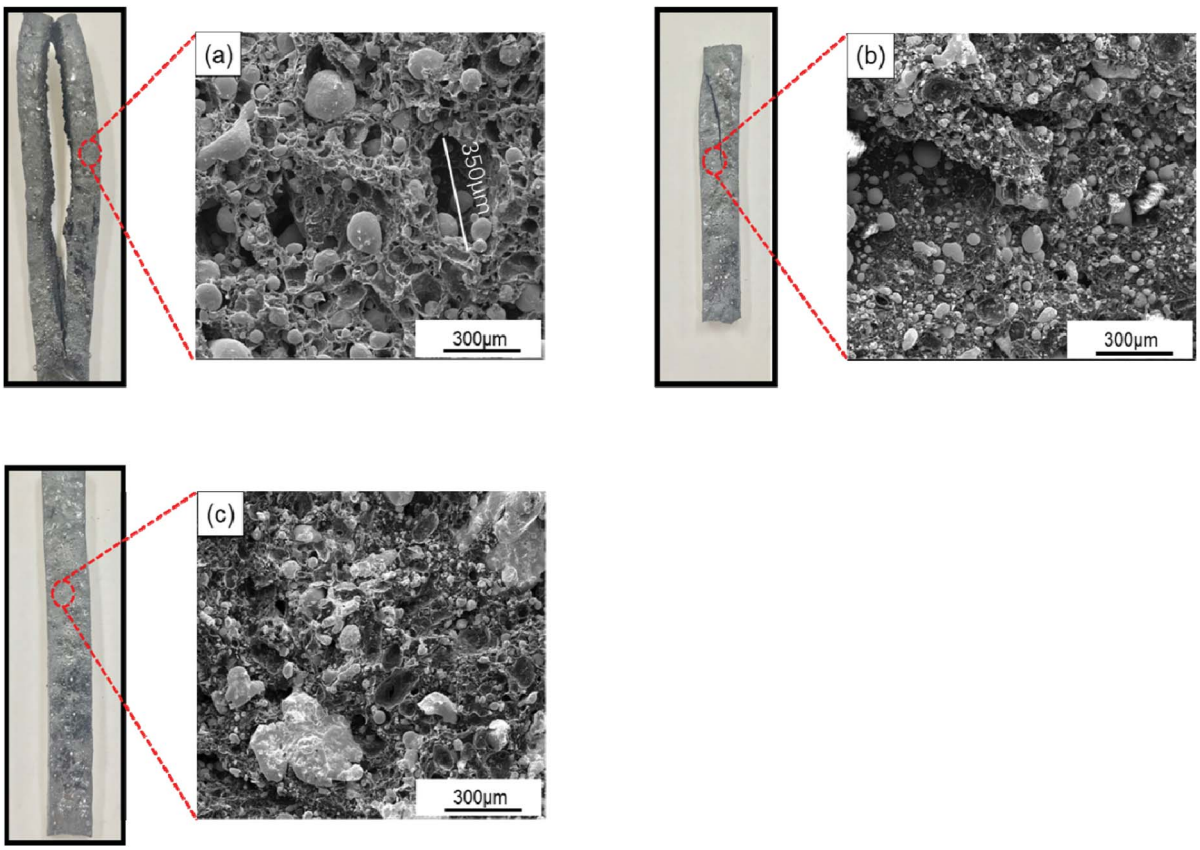

Fig. 8 Photographs and SEM images of SiO_2@Pb/B_4C/BPRs composites after burning with different content of SiO_2: (a) Pb, (b) 0.486 wt% SiO_2@Pb, (c) 0.967 wt% SiO_2@Pb.

without agglomeration. Furthermore, there are fewer holes in the composites and the cracking of composites is also improved. It can be attributed to reduction of true density difference value between fillers after coating, which is instrumental in the distribution of Pb powders in composites. With the further increase of SiO_2 content, cracks on the surface of composites disappear and solidified Pb blocks appear in the composites (Fig. 8c). This is because the SiO_2 coatings inhibit the flow of Pb liquid. The Pb liquid fills the holes and cracks to keep the structural integrity of the composites. Moreover, after solidification, it isolates the contact between oxygen and the resins to improve the composites flame retardancy.

Fig. 9 displays the mechanical properties of SiO_2@Pb/B_4C/BPRs composites with different SiO_2 content. The trend of mechanical properties of Pb/B_4C/BPRs composites reaches the maximum when the SiO_2 content is 0.237 wt% and then decreased with a further content. There are two main reasons for the improvement of mechanical properties: (1) SiO_2 increases the roughness of the surface of Pb powders, which is conducive to resin adhesion on the surface of Pb powders. In addition, OH^- groups on the surface of SiO_2 enhance the interfacial bond between Pb powders and resin. Therefore, the SiO_2 coatings reduces the gap between Pb powders and resin matrix in the microstructure, and improves the mechanical properties of the composites; (2) due to the huge density difference between Pb powders and B_4C powders, powders agglomerate in the SiO_2@Pb/B_4C/BPRs composites. There are few resins in these areas, which make it difficult to adhere to powders. Therefore, it is easy to produce cracks in these areas which lead to material fracture. After surface treatment, the density of Pb powders decrease, which is conducive to the uniform dispersion of Pb powders and B_4C powders in the composites. However, with the further increase of SiO_2 content, the specific surface area of Pb powders increases from 0.0470 to 0.4800 $m^2\ g^{-1}$ after modification. As a result, it is difficult for BPRs to coat on the surface of all powders uniformly and the BPRs coating thickness of powders surface also decreases, which lead to for the formation and propagation of internal cracks in composites. Additionally, elasticity modulus for Pb and SiO_2 are 16 GPa (ref. 32) and ~70 GPa,[33] respectively, and elasticity modulus for BPRs is very low. Thus, SiO_2 wrapped onto Pb powder surfaces increased the modulus mismatch between the Pb and BPRs. The modulus mismatch makes more prone to fine cracks at the interface under the external force.

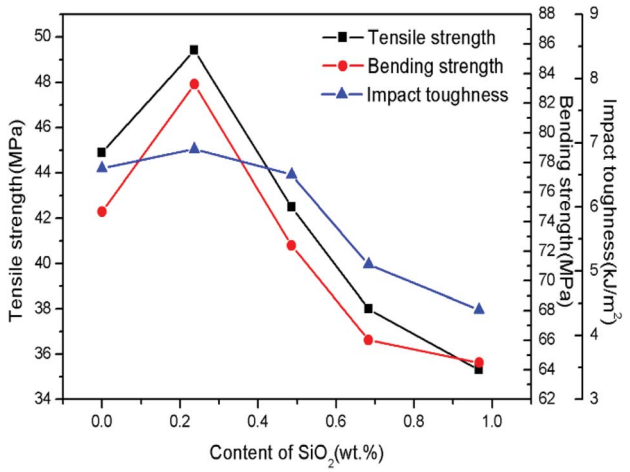

Fig. 9 Mechanical properties of SiO_2@Pb/B_4C/BPRs composites with different content of SiO_2.

4 Conclusions

In the view of the results presented in this work, the conclusions can be drawn as following:

(1) SiO_2 coated Pb powders (SiO_2@Pb) with different content can be synthesized by sol–gel method. The SiO_2 coatings on the surface of Pb powders is in flakes or islands. The specific surface area of SiO_2@Pb powders increases from 0.0470 to 0.4800 $m^2\ g^{-1}$ with the addition of SiO_2 content. Moreover, the SiO_2 coatings increase the initial oxidation temperature of SiO_2@Pb powders from 325 °C to 430 °C as thermal barriers.

(2) The SiO_2 coatings improve the interface bonding between Pb powders and BPRs and decrease the density difference between fillers, which reduce the agglomeration of fillers. Thus, the composition uniformity of SiO_2@Pb/B_4C/BPRs composites is improved after surface treatment of Pb powders, which increases the LOI, mechanical properties and decreases the thermal conductivity of SiO_2@Pb/B_4C/BPRs composites.

(3) SiO_2 coatings on Pb powders surface inhibit the agglomeration of Pb powders and the flow of molten Pb, which are beneficial for reducing voids and cracks in composites. The LOI of SiO_2@Pb/B_4C/BPRs composites increased from 41% to 42.8% with the increase of SiO_2 content.

(4) Analysing the LOI and the mechanical properties of composites, the 0.486 wt% SiO_2@Pb/B_4C/BPRs composites show the optimal comprehensive physical properties. The mechanical properties of composites prepared with 0.486 wt% SiO_2@Pb are 42.5 MPa, 72.4 MPa, 6.5 kJ m^{-2}, respectively and the LOI is 41.6%.

Conflicts of interest

There are no conflicts to declare.

Acknowledgements

This work was support by the Program for the Sichuan Key Laboratory of strategic resources application and innovation 2016sfgw001.

References

1 Y. Jiang, X. Fu, Z. Zhang, W. Du, P. Xie, C. Cheng and R. Fan, *J. Alloys Compd.*, 2019, **804**, 305–313.
2 Y. Qu, Y. Du, G. Fan, J. Xin, Y. Liu, P. Xie, S. You, Z. Zhang, K. Sun and R. Fan, *J. Alloys Compd.*, 2019, **771**, 699–710.
3 J. M. DeWitt, E. R. Benton, Y. Uchihori, N. Yasuda, E. V. Benton and A. L. Frank, *Radiat. Meas.*, 2009, **44**, 905–908.

4 D. Jóźwiak-Niedźwiedzka, K. Gibas, A. M. Brandt, M. A. Glinicki, M. Dąbrowski and P. Denis, *Procedia Eng.*, 2015, **108**, 162–169.
5 T. Xing, Y. Huang, K. Zhang and J. Wu, *RSC Adv.*, 2014, **4**, 53628–53633.
6 J. W. Shin, J.-W. Lee, S. Yu, B. K. Baek, J. P. Hong, Y. Seo, W. N. Kim, S. M. Hong and C. M. Koo, *Thermochim. Acta*, 2014, **585**, 5–9.
7 Y. Q. Tan, H. Luo, X. S. Zhou, S. M. Peng and H. B. Zhang, *RSC Adv.*, 2018, **8**, 39314–39320.
8 V. Y. Topolov and C. R. Bowen, *Mater. Lett.*, 2015, **142**, 265–268.
9 L. Li, Z. Wu, S. Jiang, S. Zhang, S. Lu, W. Chen, B. Sun and M. Zhu, *Polym. Compos.*, 2015, **36**, 892–896.
10 P. Wang, X. Zhang, G. Lim, H. Neo, A. A. Malcolm, Y. Xiang, G. Lu and J. Yang, *J. Mater. Sci.*, 2015, **50**, 5978–5992.
11 A. Bobovitch, E. Gutman, M. Schenker, L. Utevski and M. Muskatel, *Mater. Lett.*, 1995, **23**, 317–320.
12 M. A. Khattab, *J. Appl. Polym. Sci.*, 2000, **78**, 6.
13 X. Wang, M. Q. Romero, X.-Q. Zhang, R. Wang and D.-Y. Wang, *RSC Adv.*, 2015, **5**, 10647–10655.
14 C. Wu, W. Wu, H. Qu and J. Xu, *Mater. Lett.*, 2015, **160**, 282–285.
15 N. Wu and R. Yang, *Polym. Adv. Technol.*, 2011, **22**, 495–501.
16 J. Zhang, Q. Wu, G. Li, M.-C. Li, X. Sun and D. Ring, *RSC Adv.*, 2017, **7**, 24895–24902.
17 J. W. G. Takashi Kashiwagi, K. M. Butler, R. H. Harris, J. R. Shields and A. Asano, *Fire Mater.*, 2000, **24**, 277–289.
18 H. Zhong, D. Wu, P. Wei, P. Jiang, Q. Li and J. Hao, *J. Mater. Sci.*, 2007, **42**, 10106–10112.
19 L. Qomariyah, A. F. Arif, W. Widiyastuti, S. Winardi, S. Taniguchi and T. Ogi, *RSC Adv.*, 2018, **8**, 26277–26282.
20 P. Xie, Z. Zhang, K. Liu, L. Qian, F. Dang, Y. Liu, R. Fan, X. Wang and S. Dou, *Carbon*, 2017, **125**, 1–8.
21 P. Xie, Z. Zhang, Z. Wang, K. Sun and R. Fan, *Research*, 2019, **2019**, 1–11.
22 L. Martín-García, S. Ruiz-Gómez, M. Abuín, Y. Montaña, N. Carmona and L. Pérez, *RSC Adv.*, 2015, **5**, 97503–97507.
23 S. A. Mahadik, M. S. Kavale, S. K. Mukherjee and A. V. Rao, *Appl. Surf. Sci.*, 2010, **257**, 333–339.
24 F. Balas, M. Rodríguez-Delgado, C. Otero-Arean, F. Conde, E. Matesanz, L. Esquivias, J. Ramírez-Castellanos, J. Gonzalez-Calbet and M. Vallet-Regí, *Solid State Sci.*, 2007, **9**, 351–356.
25 IUPAC, *Reporting physisorption data for gas/solid systems with special reference to the determination of surface area and porosity*, 1985.
26 G. Toussaint, M. A. Rodriguez, R. Cloots, J. Rubio, F. Rubio, B. Vertruyen and C. Henrist, *J. Non-Cryst. Solids*, 2011, **357**, 951–957.
27 X. Wang, Y. Pei, M. Lu, X. Lu and X. Du, *J. Mater. Sci.*, 2014, **50**, 2113–2121.
28 T. Yamane, N. Nagai, S.-i. Katayama and M. Todoki, *J. Appl. Phys.*, 2002, 91.
29 W. Hemminger, *Int. J. Thermophys.*, 1989, **10**, 765–777.
30 A. K. Suri, C. Subramanian, J. K. Sonber and T. S. R. C. Murthy, *Int. Mater. Rev.*, 2013, **55**, 4–40.
31 J. Zhao, F. Du, W. Cui, P. Zhu, X. Zhou and X. Xie, *Composites, Part A*, 2014, **58**, 1–6.
32 D. L. Waldorf and G. A. Alers, *J. Appl. Phys.*, 1962, **33**, 3266–3269.
33 C. P. Wong and R. S. Bollampally, *J. Appl. Polym. Sci.*, 1999, **74**, 3396–3403.